International Multidisciplinary Research Journal Reviews (IMRJR)

International Multidisciplinary Research Journal Reviews (IMRJR)
A Peer-reviewed journal
Volume 2, Issue 6, June 2025
DOI 10.17148/IMRJR.2025.020601

Production and characterization of Zinc Iron Sulphide (ZnFeS) nanoparticles sourced locally from Nigeria prepared by high energy ball-milling

Azubuike Josiah Ekpunobi[1], Chiamaka Peace Onu[2*], Augustine Chukwuemeka Azubogu[3], Evangeline Njideka Onuigbo[4], Diemiruaye Mimi Jeroh[5], Overcomer Ifeanyi Anusiuba[6], Adline Nwodo[7], Emmanuel Utochukwu Ogbodo[8], Okechukwu Emmanuel Odikpo[9], Chiedozie Emmanuel Okafor[10], Adaora Lynda Ozobialu[11], Nonso Livinus Okoli[12], Chijioke Elijah Onu[13], Uche Eunice Ekpunobi[14], Chukwudi Benjamin Muomeliri[15]

Professor, Department of Physics and Industrial Physics, Nnamdi Azikiwe University Awka, Nigeria.[1]

Lecturer, Department of Physics and Industrial Physics, Nnamdi Azikiwe University Awka, Nigeria.[2]

Professor, Department of Electronics and Computer Engineering, Nnamdi Azikiwe University Awka, Nigeria.[3]

Professor, Department of Geological Sciences, Nnamdi Azikiwe University Awka, Nigeria.[4]

Lecturer, Department of Physics and Industrial Physics, Nnamdi Azikiwe University Awka, Nigeria.[5]

Lecturer, Department of Computer Sciences, Nnamdi Azikiwe University Awka, Nigeria.[6]

Post Doctoral Fellow, Magnetism and Magnetoscience Laboratory, Kagostina University, Japan.[7]

Senior Lecturer, Department of Electronics and Computer Engineering, Nnamdi Azikiwe, University Awka, Nigeria.[8]

Lecturer, Joint Universities Preliminary Examinations Board, Nnamdi Azikiwe University Awka, Nigeria.[9]

Lecturer, Department of Physics and Industrial Physics, Nnamdi Azikiwe University Awka, Nigeria.[10]

Lecturer, Department of Physics and Industrial Physics,Nnamdi Azikiwe University Awka, Nigeria.[11]

Doctoral Student, Nanoscience and Advance Materials, Federal University of ABC, Santo Andre, Sao Paulo, Brazil.[12]

Lecturer, Department of Chemical Engineering, Nnamdi Azikiwe University Awka, Nigeria.[13]

Professor, Department of Pure and Industrial Chemistry, Nnamdi Azikiwe University Awka, Nigeria.[14]

Lecturer, Department of Physics and Industrial Physics, Nnamdi Azikiwe University Awka, Nigeria.[15]

Abstract: In this work, ZnFeS nanoparticles were synthesized from its bulk material through high energy ball milling. The ZnFeS nanoparticles were sourced from Wase Local Government Area of Plateau State Nigeria, pre-treated and then ball milled. The X-ray Diffraction (XRD) was used for analyzing the structural properties and the confirmation of the nanoparticle sizes. The SEM-EDX Analysis was used to determine the morphology and elemental composition of the ZnFeS nanoparticles. The absorbance at varied wavelengths was used to evaluate the optical properties. The result showed that the ZnFeS nanoparticles have coarsed and flaked crystalline structure. The EDX results indicated the presence of zinc, sulphur and iron. The average nanoparticle size was 51.86 nm. The calculated dislocation density ranged from 0.177 x 10^{-3} nm^{-2} to 0.435 x 10^{-3} nm^{-2}. The transmittance increased as the spectrum wavelength moved from the ultraviolet region to the visible and getting up to 90% at the near-infrared region. The refractive index was found to increase as the photon energy increased from about 1.38eV to about 2.45eV. The band energy gap was 3.63eV. These properties lend credence to the potential utilization of the ZnFeS nanoparticles in diverse photovoltaic and optical instruments.

Keywords: Nanoparticles, band energy gap, optical conductivity, refractive index, absorbance

International Multidisciplinary Research Journal Reviews (IMRJR)

International Multidisciplinary Research Journal Reviews (IMRJR)
A Peer-reviewed journal
Volume 2, Issue 6, June 2025
DOI 10.17148/IMRJR.2025.020601

I. INTRODUCTION

In recent times, researchers focus more attention on nanoparticles synthesis from underutilized materials and their possible application in nanotechnology. This interest is triggered by the multi-functional properties and applications of these nanoparticles [1,2]. Nanoparticles are fine particles whose average sizes are less than 100 μm [3-5]. Recent nanotechnologies harness knowledge from physics, biotechnology, materials science and chemistry to create new materials having distinctive properties because their structures are determined on the nanometer scale [6].

Nanoparticles are the basic constituents of the nanostructure of most substances. When compared with their bulk state, the basic properties of most materials show a substantial change when converted to nano-sized particles. Furthermore, metallic bulk materials exhibit considerably different properties when compared to their nanoparticles [7]. This arises from the increase in the surface area to volume ratio resulting in the properties of the materials being determined by the surface atoms. Their small size helps to confine their electrons and produce different quantum effects. These size-dependent properties enable nanoparticles to improve both shelf life and overall electrical, mechanical, conductivity, optical and structural performance of metallic products [8-10]. Hence nanoparticles are fine particles that exhibit improved characters of the whole as a result of their properties. They have found applications in light emitting devices, solar cells, gas sensors and thin film transistors [11-15]. Nanoparticles have even reportedly been used in waste water treatment for efficient removal of reactive red azo dye [16].

The extensive use of nanoparticles is predicated on the fact that they have the necessary characteristics, which are typically distinct from bulk material. The majority of nanoparticles have a wide energy gap, good UV emissions, and a tolerable excitation binding energy [17]. Additionally, they have a high level of stability and the ability to change the electrical conductivity of gases that naturally have the potential to absorb UV rays [18-19].

Nanoparticles can be obtained via top-bottom approach and bottom-top approach. The nanoparticles in this research were obtained via top-bottom approach, in this case; milling technique. The milling technique is a top-bottom method of preparing nanoparticles. It entails breaking bulk materials into bits of sizes less than 100μm [4].

It is of two types namely: the wet milling and the dry milling. In wet milling, there is an introduction of a surface-active media that prevents the development of aggregates [20]. This can aid in uniform distribution of nanoparticles [21]. But in dry milling, the solid substance is broken down and ground as a result of friction, compression, shock, etc. It is usually solvent-free and the slow pulverizing of the particles is enhanced by the powder-to-powder friction [20]. This method is suitable for synthesizing nanoparticles of controlled length with robust interface interactions [22-23].

The ball-milling technique is a type of dry milling where the sample's chemical bonds are broken down due to the moving balls' kinetic energy (K.E.) being exerted on a much reduced material resulting in the production of nanoparticles [24-25]. Powdered particles are restricted between the inner surface of the vial and colliding balls, resulting in continuous deformation and generation of nano-sized particles with new properties and new surfaces [20, 26]. The ball-milling method has potential for easy industrial scalability in nanoparticle synthesis [27-28].

The ZnFeS nanoparticle is a zinc sulphide mineral with variable amount of iron that has huge deposit in Nigeria. Depending on the location, it may contain some trace elements such as Cd, In, Hg, Ge, Mn, Ga, and Se in varying proportions [29-33]. Hence, this work synthesized and characterized nanoparticles from ZnFeS bulk materials obtained locally in Nigeria.

II. MATERIALS AND METHODS

2.1 Material sourcing and pretreatment

The ZnFeS nanoparticles was sourced from Wase Local Government (LGA) Area of Plateau State Nigeria where there is a huge deposit of the material. It was crushed manually into smaller particles because of its bulky nature. This is to enhance the ball milling experiment.

2.2 Nanoparticle synthesis via ball milling experiment

A Planetary ball-milling machine was used to conduct the ball-milling experiment. It has vials with steel coatings and hardened steel balls within that are around 10 mm in diameter. The milling lid was used to insert the samples of the ZnFeS nanoparticles. The milling process took place at room temperature.

Throughout the procedure, a weight-to-weight ratio of 10:1 was kept between the balls and the powder. Ball-milling was done at 25 Hz using a horizontal operating approach. The milled materials were used directly with no added milling media. The ball-milling took place for a total of 10 hours, interspersed with short breaks that prevented an unwelcome

International Multidisciplinary Research Journal Reviews (IMRJR)
A Peer-reviewed journal
Volume 2, Issue 6, June 2025
DOI 10.17148/IMRJR.2025.020601

quick rise in temperature within the milling vial. After the ball-milling experiment, the milled nanoparticles were taken out and the crystal properties were used to determine the nanoparticles average size.

2.3 X-ray Diffraction (XRD)
XRD was used for analyzing the structural properties of the ZnFeS nanoparticles. The diffraction spectra were recorded at 2θ angle between 0º and 70º, Cu-target, 35Kv, 35mA and scan speed of 0.3 degree/0.02 second.

2.4 Scanning Electron Microscopy (SEM)
The surface morphology of the nanoparticles samples were obtained by SEM. Crystal shape size of the crystalline nanoparticle phase samples could be identified from the micrograph. The observation was done using a JOEL scanning electron microscope model JSM 6400. To prepare for the observation, the solid samples were placed on a brace stub sample holder using double stick carbon tape. The micrographs were recorded with 12 KV, 500x and 1000x magnification.

2.5 Crystalline properties
The crystalline size of the nanoparticles was calculated using the Debye–Scherer formula in equation 1 [34-36].

$$D = \frac{k\,\lambda}{\beta \cos\theta} \qquad (1)$$

Where D is the crystal size, K is Scherrer's constant (0.9), β is full width at half-maximum (FWHM), λ is the X-ray wavelength (0.15406nm) and θ is Bragg's diffraction angle.

2.6 Dislocation density
The dislocation density of the ZnFeS nanoparticles was calculated using equation 2

$$D_d = \frac{1}{D^2} \qquad (2)$$

Where D_d is the dislocation density and D is the crystallite size

2.7 Transmittance and reflection spectral
The transmittance of the nanoparticles was estimated from the absorbance spectrum according to equation 3 while the reflectance was evaluated using equation 4:

$$T = 10^{-A} \qquad (3)$$

$$\mathrm{R} = 1 - [\mathrm{T} + \mathrm{A}] \qquad (4)$$

where A is absorbance, R is reflectance and T is transmittance**.**

2.8 Refractive index and optical conductivity
The refractive index (R.I.) was calculated from equation 5.

$$n = \frac{1+\sqrt{R}}{1-\sqrt{R}} \qquad (5)$$

The optical conductivity was determined using equation 6.

$$\sigma = \frac{\alpha n c}{4\pi} \qquad (6)$$

where n is the R.I., R is the reflectance of the nanoparticle, σ is the optical conductivity, α is absorption coefficient, c is speed of light while π is a constant (3.142).

2.9 Extinction coefficient
The extinction coefficient (k) was evaluated from equation 7

$$k = \frac{\alpha\lambda}{4\pi} \qquad (7)$$

International Multidisciplinary Research Journal Reviews (IMRJR)
A Peer-reviewed journal
Volume 2, Issue 6, June 2025
DOI 10.17148/IMRJR.2025.020601

where α is the absorption coefficient, λ is the wavelength and π is a constant.

2.10 Dielectric constant

The dielectric constant is composed of two parts; the real and imaginary parts. The real part explains the dispersion while the imaginary part measures the rate of dissipation of the wave in the medium [37].
The real dielectric constant (ε_r) was determined using the equation 8 while the imaginary part (ε_i) was determined using equation 9.

$$\varepsilon_r = n^2 - k^2 \quad (8)$$

$$\varepsilon_i = 2nk \quad (9)$$

2.11 Energy band Gap

The energy band gap was extracted from the graph of equation 10.

$$\alpha hv = A\left(hv - E_g\right)^n \quad (10)$$

where α is the absorption coefficient, hv is the photon energy, A is a constant, E_g is the band gap, and n is for modes of transition; (1/2) for direct transition and 2 is for indirect transition).

III. RESULTS AND DISCUSSION

3.1 SEM-EDX Analysis of the Sphalerite and Monazite

Figure 2 shows the morphology of the ZnFeS nanoparticle. The ZnFeS nanoparticle was observed to be coarse, closely packed, and crystalline structured with well formed flakes and irregular edges. The result was seen to have similar morphology as reported in the literature [38].

Elemental composition was obtained using the Energy dispersive X-ray (EDX) analysis [39-40]. The EDX spectrum of ZnFeS nanoparticle is shown in figure 3. The spectrum of ZnFeS nanoparticle confirmed the presence of Zinc, Iron and Sulphide in the particle. This is in addition to the presence of Calcium, Silicon, Aluminum, etc. Some transition elements such as Germanium, Manganese, Cadmium were also detected.

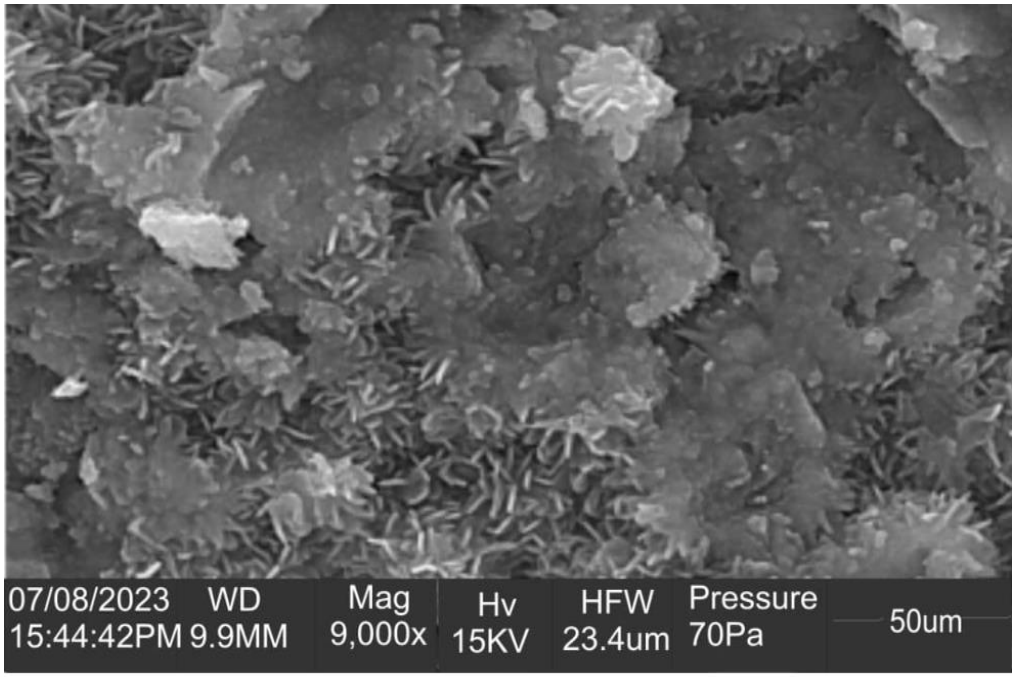

Figure 2. SEM Image of ZnFeS nanoparticle at 9000×

International Multidisciplinary Research Journal Reviews (IMRJR)
International Multidisciplinary Research Journal Reviews (IMRJR)
A Peer-reviewed journal
Volume 2, Issue 6, June 2025
DOI 10.17148/IMRJR.2025.020601

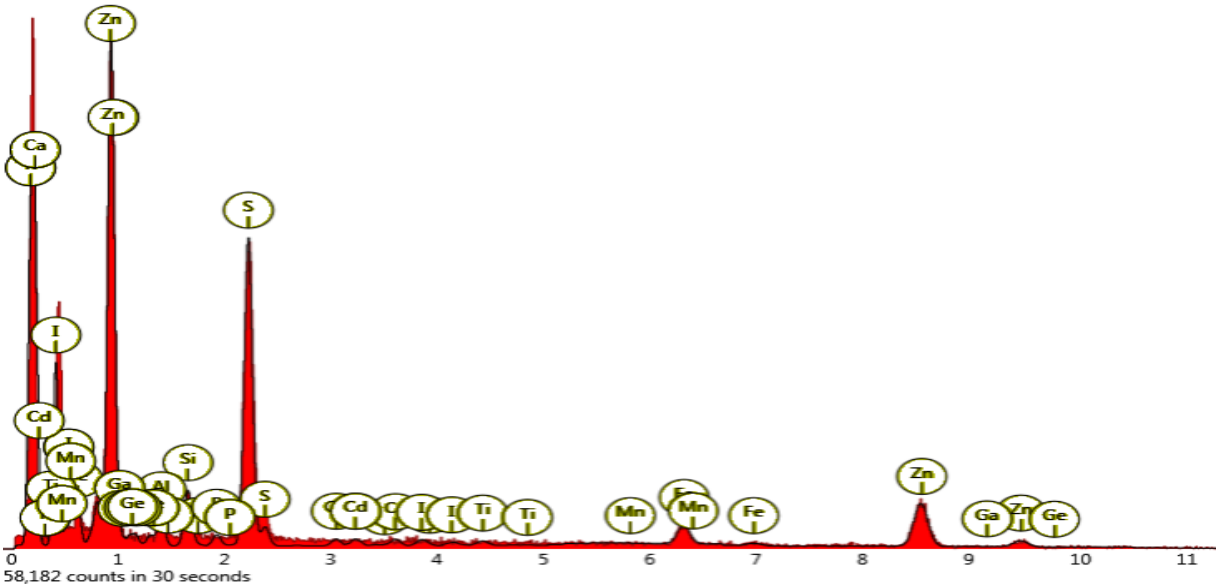

Figure 3. EDX Spectrum of ZnFeS nanoparticles

3.2 X-ray diffraction and crystal analysis

X-ray diffraction (XRD) was used in the structural and lattice analysis of the ZnFeS nanoparticles. The full width at half maximum ranged from 0.11^o to 0.49^o for ZnFeS particles. The nanoparticle spacing ranged from 1.63 to 3.44 Å. The dislocation density calculated ranged from $0.177 \times 10^{-3}\,nm^{-2}$ to $0.435 \times 10^{-3}\,nm^{-2}$ for ZnFeS nanoparticles. The dislocation density defines the number of dislocation lines per unit volume of crystals and represents the crystal defect size in a crystal. Since the dislocation density obtained is small, the nanoparticles synthesized have a high degree of crystallinity [35]. It is indirectly proportional to the particle crystalline size as it tends to decrease when the crystalline size increases. The results of some of the crystal analysis are tabulated in table 1. The crystalline size ranged from 17.44 nm to 75.26 nm for the ZnFeS nanoparticles with an average crystalline size of 51.864 nm.

Table 1. Crystal properties of the ZnFeS

20°	Lattice spacing d, (Å)	FWHM, ° (β)	Miller indices (hkl)	Crystalline size (nm)	Dislocation density $(nm)^{-2}$
25.91	3.436	0.17	100	47.95165	0.000435
28.78	3.099	0.15	110	54.67734	0.000334
30.281	2.949	0.15	110	54.86644	0.000332
32.218	2.776	0.15	110	55.12643	0.000329
32.703	2.736	0.11	110	75.26508	0.000177
33.231	2.693	0.23	110	36.04546	0.00077
38.87	2.314	0.14	111	60.17364	0.000276
42.82	2.110	0.14	200	60.95102	0.000269
43.27	2.089	0.49	200	17.44157	0.003287
47.653	1.906	0.15	210	57.89626	0.000298
56.533	1.626	0.18	211	50.11038	0.000398

The XRD pattern of ZnFeS nanoparticles is shown in Figure 4. Distinct peaks were observed at 2theta angles of 25.91^o,, 28.78^o, 30.28^o, 32.22^o, 32.70^o ,33.23^o, 38.87^o, 42.82^o, 43.27^o, 47.65^o and 56.53^o which correspond to miller indices of 100, 110, 110, 110, 110, 111, 200, 200, 210, and 211 respectively on the crystallographic planes [41-42]. Insignificant broad peaks were observed in the pattern indicating little impurities within the crystal structure. The effect of impurities on the crystal structure has a significant role in the change of the physical properties [43].

International Multidisciplinary Research Journal Reviews (IMRJR)
International Multidisciplinary Research Journal Reviews (IMRJR)
A Peer-reviewed journal
Volume 2, Issue 6, June 2025
DOI 10.17148/IMRJR.2025.020601

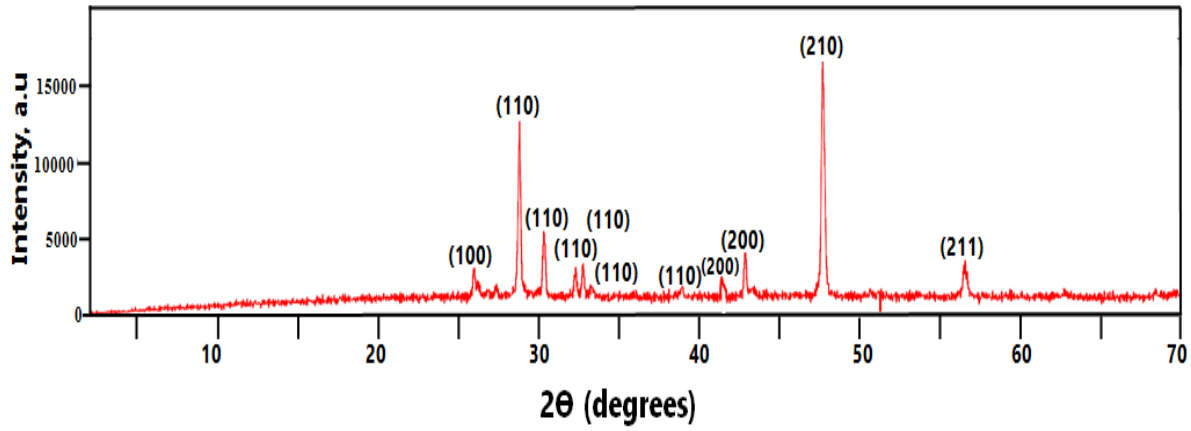

Figure 4. X-ray diffraction pattern of ZnFeS nanoparticles

3.3 Absorption and transmittance spectra

Figure 5 shows the absorption spectrum of the ZnFeS nanoparticles with distilled water as the dispersing agent (SDW) and ZnFeS particles with ethanol as the dispersing agent (SET). The samples showed relatively low absorbance (of 22 to 36%) at ultraviolet wavelengths (200 to 400 nm). The absorbance decreased at increased wavelengths [44]. An initial steep reduction between 600 nm to 700 nm was observed throughout the samples. The absorbance of the whole samples also experienced irregular reduction towards the visible region and the near-infrared regions. The absorbance was almost zero at the near-infrared regions (within 10% to 1%). This indicates that the ZnFeS nanoparticles are non-absorbing at the near-infrared regions. Similar trend has been reported [18, 45-46]. The distilled water dispersed particle showed similar absorbance with the ethanol dispersed particle at both the ultraviolet and near-infrared regions. However, at some wavelengths, the absorbance of the distilled water dispersed particles was marginally higher than that of the ethanol dispersed particles.

The transmittance spectrum is depicted in figure 6. The transmittance showed an increase from around 45% to 60% in the ultraviolet region about 90% to the visible region and then to the near-infrared region. Similar trend has been reported [47]. The high transmittance in the visible region indicates the potential easy photon passage and hence likely suggesting applicability of ZnFeS nanoparticles in electron transport layers of optical materials [48]. The decreased transmittance in the UV region results from enhanced scattering of photons by crystal defects within the near infrared region [49].

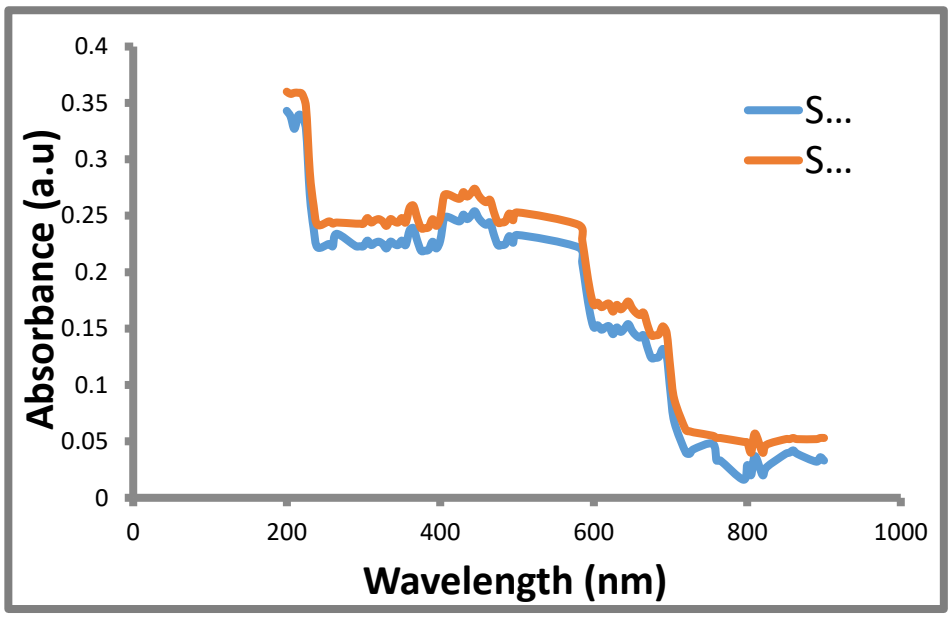

Figure 5. Absorbance spectrum of the ZnFeS nanoparticles.

International Multidisciplinary Research Journal Reviews (IMRJR)
A Peer-reviewed journal
Volume 2, Issue 6, June 2025
DOI 10.17148/IMRJR.2025.020601

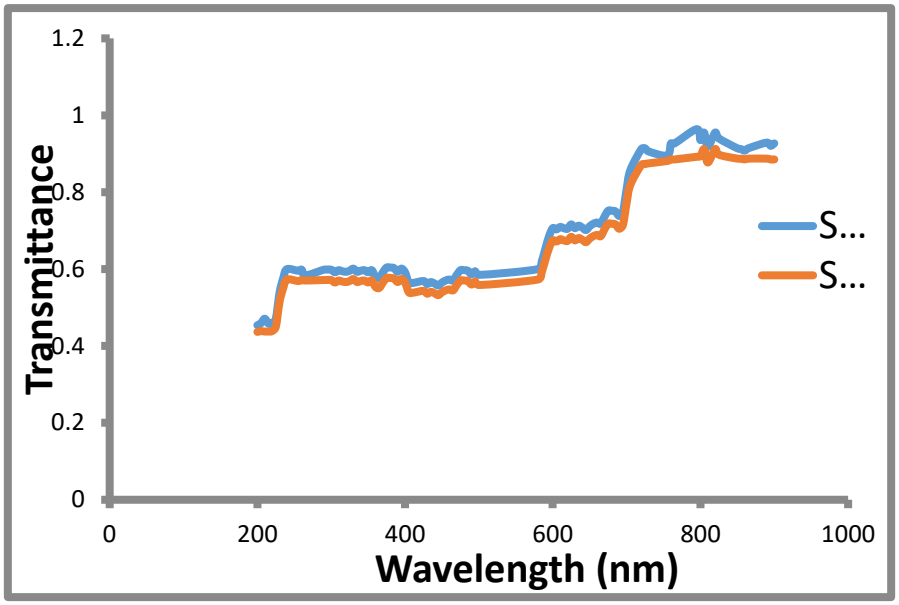

Figure 6. Transmittance spectrum of the ZnFeS nanoparticles.

3.4 Reflectance and refractive index

The reflectance was depicted as a function of wavelength in Figure 7. Figure 7 indicates a slight increase in the reflectance from about 17.1 to 19.9% in the ultraviolet region and further reduced from 19.9% to 4.1% in the visible region in line with the report of [50]. Towards the NIR, a sharp reduction from 4.1 to 3.9% was observed. The poor reflectance observed throughout the regions of the spectrum suggests the possibility of its application in the window layer component of a solar cell. The nature of the plot compares with previous report [51]. Very low reflectance is desired for optical applications [52], suggesting the ZnFeS nanoparticles a desired material for optical applications.

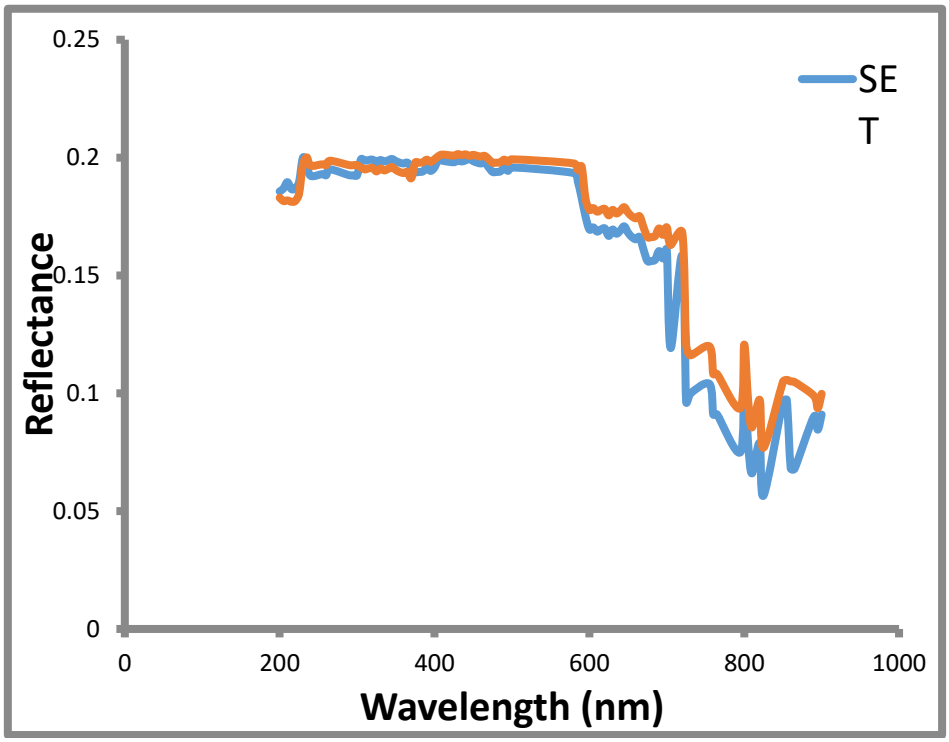

Figure 7. Reflectance of the ZnFeS nanoparticles

International Multidisciplinary Research Journal Reviews (IMRJR)
A Peer-reviewed journal
Volume 2, Issue 6, June 2025
DOI 10.17148/IMRJR.2025.020601

The refractive index is expressed as a function of photon energy in figure 8.

The refractive index was found to increase steeply as the photon energy increased from about 1.38eV to about 2.45eV and then experienced relative stability as the photon energy increased to about 2.49eV to 2.64eV. This indicates that the refractive index of the ZnFeS nanoparticles can be tuned to manipulate their matrix characteristics even at molecular stage [53]. Refractive index depends on wavelength and moderates the interaction between the nanoparticles and light in various applications [54]. The refractive index is a major physical parameter used to evaluate the quality of nanoparticle-based solids [53].

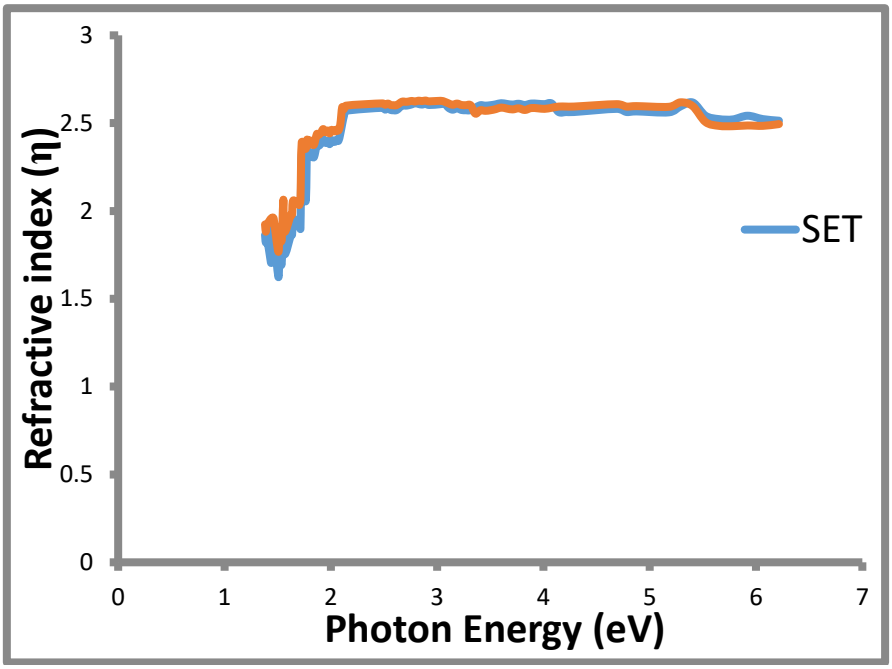

Figure 8. Refractive index of the ZnFeS nanoparticles

3.5 Absorption coefficient and extinction coefficient

The plot of absorption coefficient is presented in figure 9.

The absorption coefficient describes the ability of the nanoparticles to absorb light. In figure 9, there was an observed high absorption coefficient in the UV region. However, a reduction in the absorption coefficient of the ZnFeS nanoparticles was observed as the wavelength increased. At the near-infrared region, the absorption coefficient was almost constant with further increase in the wavelength. The high absorption coefficient of the ZnFeS nanoparticles in the ultraviolet region indicates their capacity to absorb light within the UV region [55].

The plot of extinction coefficient against wavelength is displayed in figure 10. An initial steep reduction in the extinction coefficient was observed at the ultraviolet region which then gradually decreases towards the visible region. Since nanoparticles are not monodispersed, the determination of the molar concentration can be achieved through the evaluation of the extinction coefficient which is a primary parameter in calculating the nanoparticle concentration [56]. Furthermore, relatively high extinction coefficient denotes ability to dissipate absorbed energy spontaneously as heat and not as detrimental radiation [57].

International Multidisciplinary Research Journal Reviews (IMRJR)
A Peer-reviewed journal
Volume 2, Issue 6, June 2025
DOI 10.17148/IMRJR.2025.020601

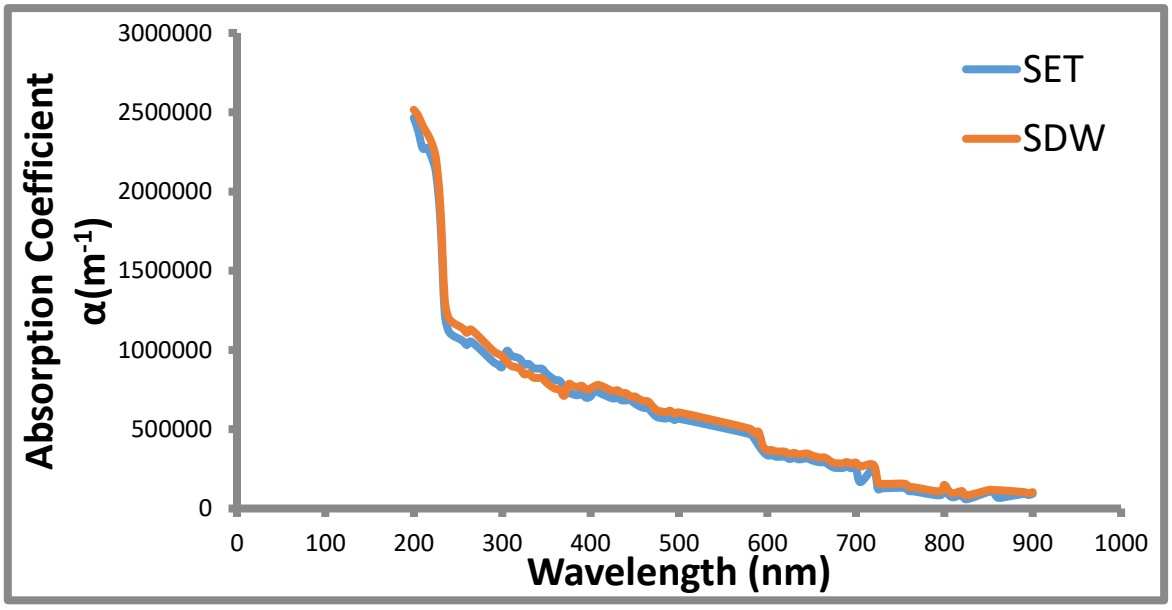

Figure 9. Plot Absorption Coefficient of the ZnFeS nanoparticles

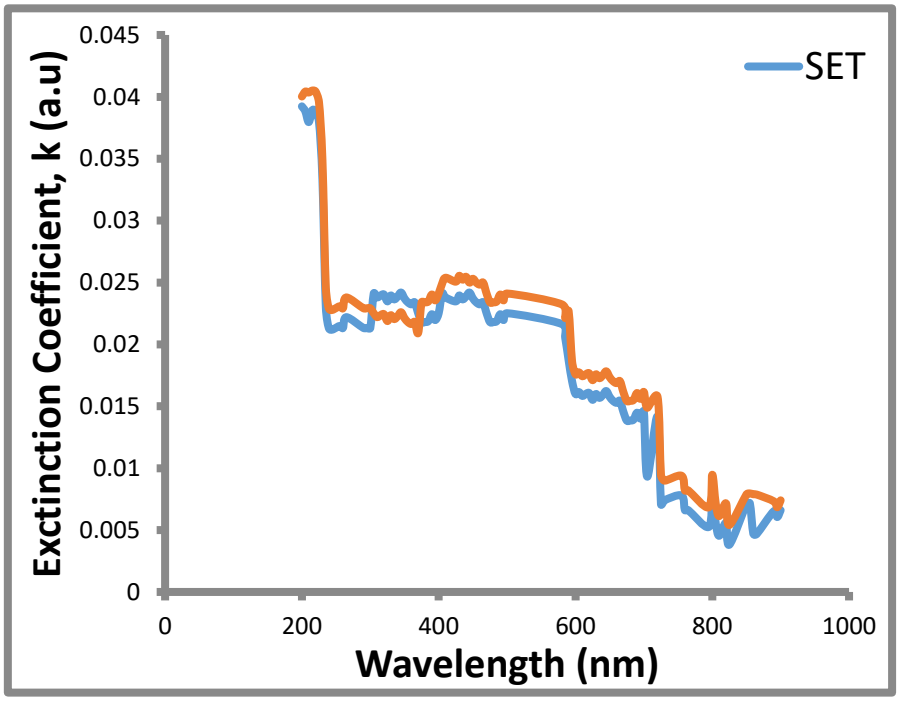

Figure 10. Plot of Extinction Coefficient of ZnFeS nanoparticles

3.6 Dielectric constant

The plot of the real and imaginary parts of the dielectric constant as a function of photon energy are shown in figures 11 and 12 respectively.

A steep and relatively unsteady increase in the real dielectric constant was observed with increase in the photon energy up to about 2.4eV which then stabilizes till about 5.6eV before experiencing a slight increase again. The real part of the dielectric constant relates to the dispersion and polarization of the material [37].

Imaginary dielectric constant is a direct function of the extinction coefficient and the refractive index. The data on the real and imaginary parts of the dielectric constant provide knowledge concerning the loss factor, which is the ratio between the imaginary and real parts of the dielectric constant [58].

International Multidisciplinary Research Journal Reviews (IMRJR)
A Peer-reviewed journal
Volume 2, Issue 6, June 2025
DOI 10.17148/IMRJR.2025.020601

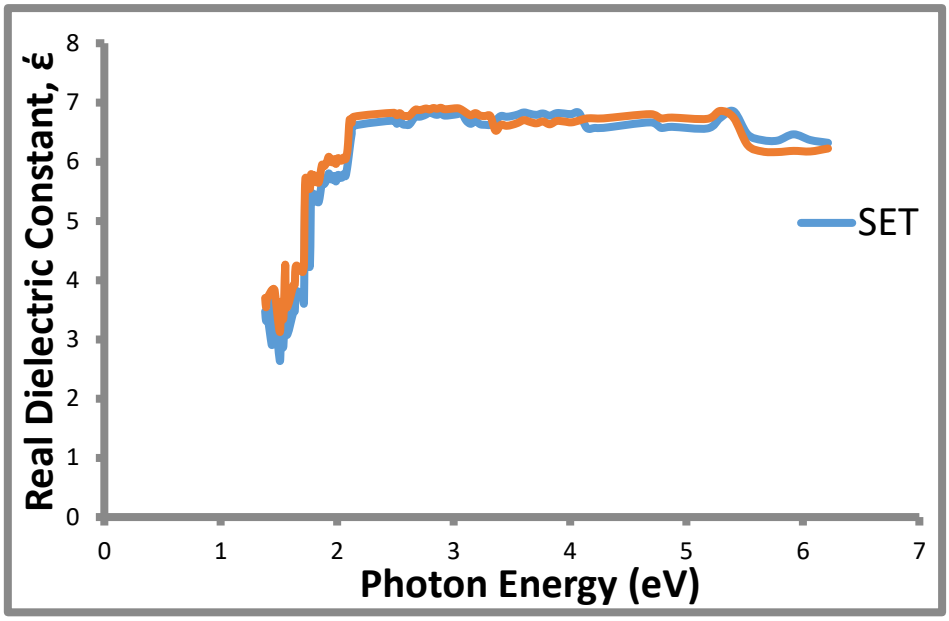

Figure 11. Plot of Real part Dielectric Constant

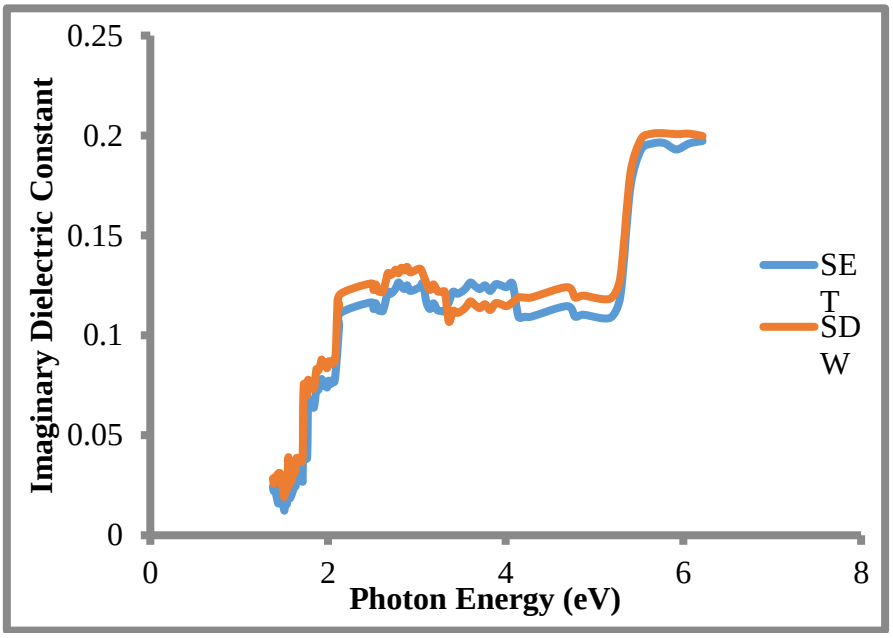

Figure 12. Plot of Imaginary Dielectric Constant

3.7 Optical conductivity

The plot of the optical conductivity against the photon energy is presented in figure 13. The optical conductivity of the ZnFeS nanoparticles was determined as a function of absorption coefficient and the refractive index of the material [59]. The optical conductivity experienced an almost linear increase as the photon energy increased from 1.46eV to about 3.9eV. At relatively higher photon energy of above 4.0eV, the increase of the optical conductivity with the photon energy was irregular. The optical conductivity plays a huge role in evaluating the particle's atomic structure and connects the current density to the material's exposure to different wavelengths of light in the electric field. It also serves as the basis for determining the spectra of some nanoparticles [60].

International Multidisciplinary Research Journal Reviews (IMRJR)
A Peer-reviewed journal
Volume 2, Issue 6, June 2025
DOI 10.17148/IMRJR.2025.020601

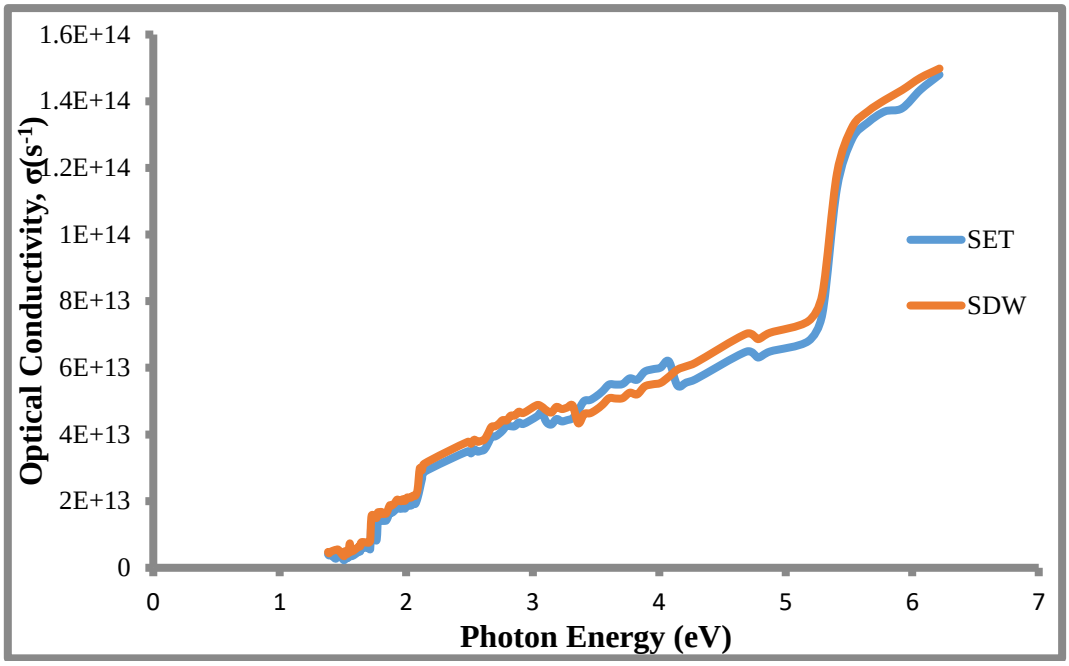

Figure 13. Plot of the Optical Conductivity of the ZnFeS nanoparticles

3.8 Band energy

The band energy gap is the minimum quantity of energy needed to excite an electron to a state where it can conduct in the condition band. It is a major parameter used in the design of optoelectronic instruments [59]. Figures 14 and 15 are the plots of plot of $(\alpha h\nu)^2$ versus photon energy for the ZnFeS nanoparticles dispersed in ethanol and distilled water respectively . The band energy gap was determined by exploiting the tangential line of the plot of $(\alpha h\nu)^2$ versus photon energy [2]. The band energy obtained was 4.96eV and 3.63eV for the ethanol dispersed and distilled water dispersed respectively, this agrees with the work done by [61]. The band energy of the ZnFeS particles dispersed in ethanol was slightly higher to that disperse in distilled water.

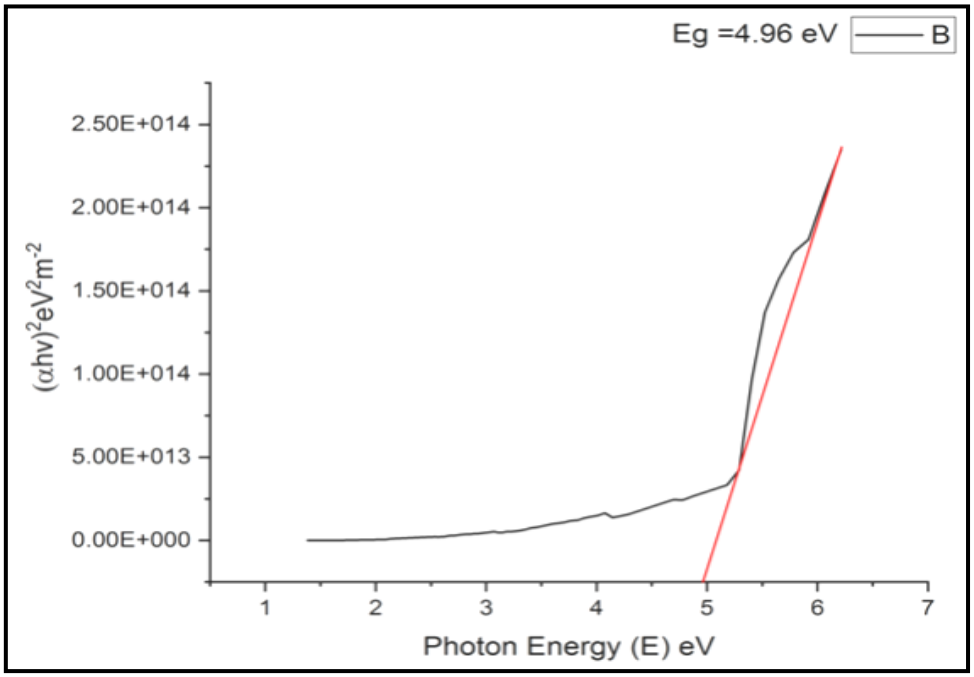

Figure 14. Band gap energy of Ethanol dispersed ZnFeS nanoparticles.

International Multidisciplinary Research Journal Reviews (IMRJR)
A Peer-reviewed journal
Volume 2, Issue 6, June 2025
DOI 10.17148/IMRJR.2025.020601

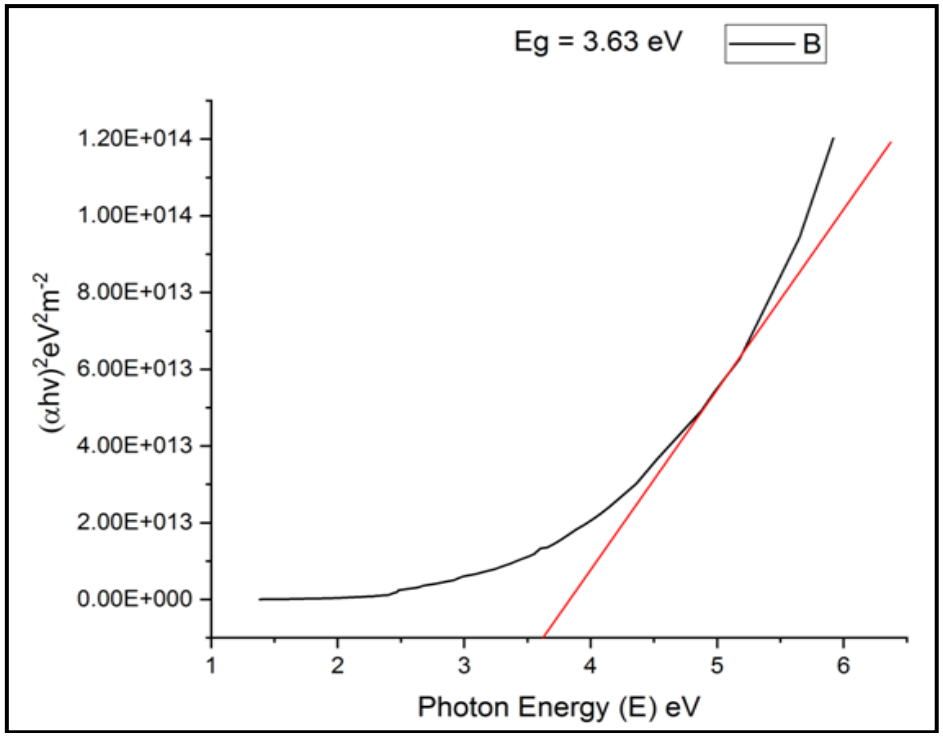

Figures 15. Band gap energy of ZnFeS nanoparticles dispersed by Distilled water.

IV. CONCLUSION

Nanoparticles were synthesized from bulk Sphalerite materials and characterized. High energy ball milling technique was used to prepare the nanoparticles. Various characterization techniques such as XRD, SEM-EDX, and Absorbance were used to determine the properties. The SEM results showed the coarsed nature of the Sphalerite. The nanoparticle size ranged from 17.44nm to 75.26nm while the dislocation density calculated ranged from 0.177 x 10^{-3} nm^{-2} to 0.435 x 10^{-3} nm^{-2}. High transmittance was observed in the visible region which indicated the potential easy photon passage. The optical conductivity experienced an almost linear increase as the photon energy increased from 1.46eV to about 3.9eV.

ACKNOWLEDGEMENT

This research was supported by TETFUND, with the reference number TETF/DR&D-CE/NRF 2021/SETI/ICT/00034/01

REFERENCES

[1] Onu, C. P., Ekpunobi, A. J., Okafor, C. E., Ozobialu, L. A., (2023). Optical Properties of Monazite Nanoparticles Prepared Via Ball Milling. *Asian Journal of Research and Reviews in Physics 7(4) 17-29, 2023;*. DOI: 10.9734/AJR2P/2023/v7i4146
[2] Faramawy, A., Elsayed, H., Scian, C., and Mattei, G., (2022). Structural, Optical, Magnetic and Electrical Properties of Sputtered ZnO and ZnO:Fe Thin Films: The Role of Deposition Power. *Ceramics*, 5, 1128–1153. https://doi.org/10.3390/ceramics5040080.
[3] Ndukwe, F. O. and A. J. Ekpunobi (2023) Processing and Characterization of Limestone Nanoparticles. *American Journal of Physical Sciences* 1 (1) 4 : 63 - 70, 2023
[4] Mhadhbi, M., (2021). Modelling of the High-Energy Ball Milling Process. *Advances in Materials Physics and Chemistry*, 11, 31-44. https://doi.org/10.4236/ampc.2021.111004
[5] Prerna, K., Anubhav, D., and Ratan, G., (2021). Nanoparticles: An Overview Drugs and Cell Therapies in Haematology (ISSN: 2281-4876) 10, (1), 1487 – 1497.
[6] Mobasser, S. H., and Firoozi, A. A. (2016). Review of Nanotechnology Applications in Science and Engineering. J. Science line Publication Journal of Civil Engineering and Urbanism6, (4): 84-93.
[7] Satoshi, H., and Nick, S., (2013). Introduction to Nanoparticles. Microwaves in Nanoparticle Synthesis, First Edition. 1 – 24.

International Multidisciplinary Research Journal Reviews (IMRJR)
A Peer-reviewed journal
Volume 2, Issue 6, June 2025
DOI 10.17148/IMRJR.2025.020601

[8] Kaur, N., Kaur, S., Singh, J., and Rawat, M., (2016). A Review on Zinc Sulphide Nanoparticles: From Synthesis, Properties to Applications. J Bioelectron Nanotechnol.,1(1): 5.
[9] Loutfy, H.M., (2019). Nanoelectronic Materials Fundamentals and Applications. *Advanced Structured Materials*. https://doi.org/10.1007/978-3-030-21621-4.
[10] Nwauzor, J. N., Ekpunobi, A. J., Babalola, A. D. (2023) Processing and Characterization of Iron Oxide Nanoparticle Produced by Ball Milling Technique. *Asian Journal of Physical and Chemical Sciences* 11 (1) 27-35, DOI: 10.9734/AJOPACS/2023/v11i1193
[11] Theerthagiri, J., Salla, S., Senthil, R.A., Nithyadharseni, P., Madankumar, A., Arunachalam, P., Maiyalagan, T., and Kim, H.S., (2019) A review on ZnO nanostructured materials: Energy, environmental and biological applications. *Nanotechnology*, 30, doi:10.1088/1361-6528/ab268a 392001.
[12] Hwang, D.K., Oh, M.S., Lim, J.H., and Park, S.J. (2007) ZnO thin films and light-emitting diodes. J. Phys. D Appl. Phys. 2007, 40, R387–R412. DOI 10.1088/0022-3727/40/22/R01
[13] Hamid, S.B.A., Teh, S.J., and Lai, C.W. (2017) Photocatalytic Water Oxidation on ZnO: A Review. Catalysts, 7, 93. 1 – 14. doi:10.3390/catal7030093
[14] Tereshchenko, A., Bechelany, M., Viter, R., Khranovskyy, V., Smyntyna, V., Starodub, N., and Yakimova, R., (2016) Optical biosensors based on ZnO nanostructures: Advantages and perspectives. A review. Sens. Actuators B Chem., 229, 664–677.https://doi.org/10.1016/j.snb.2016.01.099
[15] Kumar, R., Kumar, G., Al-Dossary, O., and Umar, A., (2015) ZnO nanostructured thin films: Depositions, properties and applications—A review. Mater. Express 2015, 5, 3–23. doi:10.1166/mex.2015.1204
[16] Wei, X., Wang, X., Bin Gao, Weixin Zou, Lin Dong (2020) Facile Ball-Milling Synthesis of CuO/Biochar Nanocomposites for Efficient Removal of Reactive Red 120. ACS Omega2020,5,5748-5755. https://dx.doi.org/10.1021/acsomega.9b03787
[17] Rong, P., Ren, S., and Yu, Q., (2018). Fabrications and Applications of ZnO Nanomaterials in Flexible Functional Devices-A Review. Crit. Rev. Anal. Chem., 49, 336–349. https://doi.org/10.1080/10408347.2018.1531691.
[18] Madkhali, N., (2022). Analysis of Structural, Optical, and Magnetic Properties of (Fe,Co) Co-Doped ZnO Nanoparticles Synthesized under UV Light. Condens. Matter, 7, 63.https://doi.org/10.3390/condmat7040063
[19] Liu, X., Pan, L., Zhao, Q., Lv, T., Zhu, G., Chen, T., Lu, T., Sun, Z., and Sun, C., (2011). UVassisted photocatalytic synthesis of ZnO–reduced graphene oxide composites with enhanced photocatalytic activity in reduction of Cr(VI). Chem. Eng. Journal, 183, 238–243. doi: 10.1016/j.cej.2011.12.068.
[20] Joy, J., Krishnamoorthy, A., Tanna, A., Kamathe, V., Nagar, R., and Srinivasan, S., (2022). Recent Developments on the Synthesis of Nanocomposite Materials via Ball Milling Approach for Energy Storage Applications. Appl. Sci. https://doi.org/10.3390/app12189312.
[21] Bor, A., Jargalsaikhan, B., Lee, J., and Choi, H., (2020). Effect of Different Milling Media for Surface Coating on the Copper Powder Using Two Kinds of Ball Mills with Discrete Element Method Simulation. Coatings, 10, 898.
[22] Verma, R., Rathod, M., and Goyal, R., (2021). Effect of milling parameters on EMI shielding of the PES/MWCNT nanocomposites. Mater. Today Proc., 43, 3169–3172.
[23] Restivo, J., Orge, C.A., Santos, A.S.G., Soares, O.S.G., and Pereira, M.F.R., (2022). Nano- and macro-structured cerium oxide–Carbon nanotubes composites for the catalytic ozonation of organic pollutants in water. Catal. Today, 384–386, 187–196.
[24] Carmen, C.P., Susana, F. B., and Wim, M. D.,(2019). Ball milling: a green technology for the preparation and functionalisation of nanocellulose derivatives. Nanoscale Adv., 1, 937. DOI: 10.1039/c8na00238j.
[25] Tan, X., Jaka, S., Wenrong, Y.,Yongbai, Y., Alexey, M., Glushenkov, Lu, H.L., ,Patrick, C., Howlettb, and Ying, C., (2013) Ball milling: a green mechanochemical approach for synthesis of nitrogen doped carbon nanoparticles. Nanoscale, 5, 7970. DOI: 10.1039/c3nr02328a.
[26] Rijesh, M., Aswin, D., Kapil, D.,. Surendranathan, A. O., and Sreekanth, M. S., (2018). Effect of Milling Time on Production of Aluminium Nanoparticle by High Energy Ball Milling, *International Journal of Mechanical Engineering and Technology*, 9(8), 646–652.
[27] Zhang, N., Mao, Y., Wu, S., and Xu, W., (2022). Effects of the Ball Milling Process on the Particle Size of Graphene Oxide and Its Application in Enhancing the Thermal Conductivity of Wood. *Forests* 13, 1325. https://doi.org/10.3390/f13081325.
[28] Alami, A.H., Aokal, K., Olabi, A.G., Alasad, S., and Aljaghoub, H., (2021). Applications of graphene for energy harvesting applications: Focus on mechanical synthesis routes for graphene production. Energy Sources Part A Recovery Util. Environ. Eff. 43, 1–30.
[29] Li, L., Han, R., Zhang, Y., Wu, J., and Feng, Z., (2022). Trace element signatures of sphalerite in the Sichuan Daliangzi Gerich Pb-Zn deposit and its implications for deep ore prospecting. Front. Earth Sci. 10:928738. doi: 10.3389/feart.2022.928738
[30] Sokol, E.V., Kokh, S.N., Nekipelova, A.V., Abersteiner, A., Seryotkin, Y.V., Ershov, V.V., Nikitenko, O.A., and Deviatiiarova, A.S., (2021). Ge-Hg-Rich Sphalerite and Pb, Sb, As, Hg, and Ag Sulfide Assemblages in Mud Volcanoes of Sakhalin Island, Russia: An Insight into Possible Origin. *Minerals*, 11, 1186. https://doi.org/10.3390/min11111186

[31] Damian, G., Buzatu, A., Apopei, A.I., Damian, F., and Maftei, A.E., (2021). Hydrothermal Sphalerites from Ore Deposits of Baia Mare Area. *Minerals*, 11, 1323. https://doi.org/ 10.3390/min11121323.
[32] Dincˇa, G., Apopei, A.I., Szabo, R., and Maftei, A.E., (2022). The Effect of Mn Substitution on Natural Sphalerites by Means of Raman Spectroscopy: A Case Study of the Săcărâmb Au–Ag–Te Ore Deposit, Apuseni Mountains, Romania. *Minerals*, 12, 885. https://doi.org/10.3390/min12070885.
[33] Baˇcík, P., Fridrichová, J., Rybnikova, O., Štubˇna, J., Illášová, L'., Škoda, R., Vaculoviˇc, T., Pulišová, Z., and Seˇckár, P., (2023). Crystal-Chemical and Spectroscopic Study of Gem Sphalerite from Banská Štiavnica, Slovakia. *Minerals*, 13, 109. https://doi.org/10.3390/ min13010109.
[34] Ashraf, R., Saira R., Zohra N.K., and Shahzad N., (2015). Structural and magnetic properties of iron doped ZnO nanoparticles. *Materials Today*: Proceedings 2, 5384 – 5389 doi:10.1016/j. matpr.2015.11.055.
[35] Sutapa, I.W., Abdul W.W., Taba, P., and Nafie N. L., (2018). Dislocation, crystallite size distribution and lattice strain of magnesium oxide nanoparticles. IOP Conf. Series: *Journal of Physics: Conference Series* (979)012021 doi :10.1088/1742- 6596/979/1/012021.
[36] Ottih, I. E., Ekpunobi, A. J., P. I. Ekwo (2011) structural and optical properties of chemical bath deposites zinc nickel sulphide (ZnNiS) thin films. *Moldavian Journal of the Physical Sciences*, 10 (2) 194 – 200
[37] Yakuphanoglu F., Barim G., and Erol I. (2007). The effect of $FeCl_3$ on the optical constants and optical band gap of MBZMA-CO-MMA polymer thin films. *Physica B*, 391, 136-140.
[38] Granados J.A., Reyez M,P., Teja A.M., Palacois E.G., Perez M.L., Barrientos F.R., Juarez J.C., and Cobos J.A., (2020). Characterization by FTIR of Sphalerite obtained in the floatation without collector in the presence of Ferric Iron. *The Minerals, Metals and Material Society*. DOI: http//doi.org/10.007/978-3-030-36628-5_44.
[39] Kang, X., Yirong, X., Xuyang, C., Hao, X., and Yufang, L., (2022). Advanced characterization of membrane surface fouling. *Principles, New Materials, Modelling, Characterization and Applications* 499-532. https://doi.org/10.1016/B978-0-323-89977-2.00022-1.
[40] Dengo, N., Vittadini, A., Natile, M. M., and Gross, S. (2020). In-depth study of ZnS nanoparticle surface properties with a combined experimental and theoretical approach. *The Journal of Physical Chemistry C, 124*(14), 7777-7789.
[41] Mbonu, J. I. (2015) Determination of Ni(II) crystal structure by powder x-ray diffraction. *Scientia Africana*, 14 (1), 158-164.
[42] Falak, S. (2010) Crystal Structure Determination I. *Pakistan Institute of Engineering and Applied Sciences* 1 – 41.
[43] Saleem A. H., Rashid O. K., and Sura N.T. (2016). Structural and optical properties of Tin Oxide and Indium doped SnO_2 thin films deposited by thermal evaporation technique. *Journal of Advances in Physics*, 12 (3), 4394-4399.
[44] Ezenwa I.A, Ekpunobi A. J. (2011) Optical properties and band offsets of cds/zns superlattice deposited by chemical bath. *Journal of Non-Oxide Glasses* 3 (3), 77-87
[45] Carofiglio, M., Laurenti, M., Vighetto, V., Racca, L., Barui, S., Garino, N., Gerbaldo, R., Laviano,F.,and Cauda, V., (2021). Iron-Doped ZnO Nanoparticles as Multifunctional *Nano platformsforTheranostics. Nanomaterials* 11, 2628.https://doi.org/10.3390/nano11102628.
[46] Khalid N.R., Hammad A., Tahir M.B., Rafique M., Iqbal, T., Nabi, G., and Hussain M.K., (2019) Enhanced photocatalytic activity of Al and Fe co-doped ZnO nanorods for methylene blue degradation. *Ceramics International* (45) 21430–21435, https://doi.org/10.1016/j.ceramint.2019.07.132.
[47] Gao, P., Yin, X.S., Zhao, S.F., Wu, Z.H., Ren, S.P., Fei, S.G., (2013). Wrinkle like design of notch filter. *Optical Instruments* 35, 82–90 (in Chinese)
[48] Khalid M., Sacid S., and Muhammed T. (2017). Current Status of electron transport layers in perovskite Solar Cells: materials and properties. *RSC Advances*, 28(7), 17044-17062.
[49] Simon K. O., Ekpunobi, A. J., , Imosobomeh L. Ikhioya (2022) Synthesis and Characterization of ZnS Nanoparticles by Ball Milling Technique. *SSRG International Journal of Material Science and Engineering* 8 (3), 6-13, https://doi.org/10.14445/23948884/IJMSE-V8I3P102
[50] Okafor C. E., Okoli D. N., Imosobomeh L. I. (2022) Effect of Doping and Co-sensitization on the Photovoltaic Properties of Natural Dye-sensitized Solar Cells. *SSRG International Journal of Applied Physics* 9 (3), 44-54, https://doi.org/10.14445/23500301/IJAP-V9I3P105
[51] Nada, M., (2010). Structural and Optical Properties of ZnS Thin Films Prepared by Spray Pyrolysis Technique, Department of Physics, College of Science, University of Baghdad, Baghdad-Iraq.
[52] Wanjala, K. S., Njoroge, W. K., and Ngaruiya, J. M. (2016). Optical and electrical characterization of ZnS: Sn thin films for solar cell application. Int. J. Energy Enginneering, 6(1).
[53] Hiroshi K., Ayumu I., Katja O., Ilpo N., (2016) Refractive index measurement of nanoparticles by immersion refractometry based on a surface plasmon resonance sensor. *Chemical Physics Letters*, (654), 72-75. https://doi.org/10.1016/j.cplett.2016.05.013
[54] Edwin V.D.P., Frank, A.W.C., Auguste S., Rienk N., and Ton G.V.L., (2014) Refractive Index Determination of Nanoparticles in Suspension Using Nanoparticle Tracking Analysis. *ACS Nano Letter.*, 14, 11, 6195–6201. dx.doi.org/10.1021/nl503371p.

International Multidisciplinary Research Journal Reviews (IMRJR)
A Peer-reviewed journal
Volume 2, Issue 6, June 2025
DOI 10.17148/IMRJR.2025.020601

[55] Oluyamo S.S., and Agunbiade D.B., (2016). Spin coated Tin oxide thin film for optical and optoelectronic materials application. *International Journal of innovated Research and Advanced studies (IJIRAS)*,3(8), 394-398.
[56] Liu X., Mark A., Jinhai W., and Qun H., (2007b). Extinction coefficient of gold nanoparticles with different sizes and different capping ligands. *Colloids and Surfaces B: Biointerfaces* (58) 3–7. doi:10.1016/j.colsurfb.2006.08.005'
[57] Kröhnke, C., (2001) Encyclopedia of Materials: Science and Technology. Elsevier Publishers.
58] Noor H., Majeed A.H., and Ahmed H., (2019) Structural, Optical and Dielectric Properties of (PS-In2 O3 / ZnCoFe2 O4) Nanocomposites. *Egyptian Journal of Chemistry*. Egypt. J. Chem. V62(2),577 – 592. DOI: 10.21608/ejchem.14646.1887.
[59]Al-Hammadi A. H., and Sadiq H. K., (2023) Investigations on Optical and Electrical Conductivity of Ba/Ni/Zn/Fe16O27 Ferrite Nanoparticles. *Biointerface Research in Applied Chemistry*. 13 (2) 168 https://doi.org/10.33263/BRIAC132.168.
[60] Koval, A. O. (2022) Optical Conductivity of Spherical Metal Nanoparticles Taking into Account the Size Dependence of the Fermi Energy. *Journal of nano and electronic physics*. 14 (2)doi: 10.21272/jnep.14(2).02013
[61] Edelbro R., Sandstrom A., and Paul J., (2003). Full Potential Calculation of Electron band structures of Sphalerite, Pyrites and Chalcopyrite. *Applied Surface Science*, www.elsevier.com. (206), 300 – 313. DOI: 10.1016/50169-4332(02)01284-9.